Influence of the Grain Size on the Conduction Mechanism of Barium Strontium Titanate Thin Films

Ala'eddin A. Saif, Zul Azhar Zahid Jamal, and Prabakaran Poopalan

Microfabrication Cleanroom, School of Microelectronic Engineering, University Malaysia Perlis (UniMAP), Kuala Perlis, 02000, Perlis, Malaysia

Reprint requests to A. A. S.; Tel.: +60 19 4948919, E-mail: alasaif82@hotmail.com

Z. Naturforsch. **66a,** 784 – 790 (2011) / DOI: 10.5560/ZNA.2011-0040
Received February 1, 2011 / revised July 28, 2011

Sol-gel barium strontium titanate ($Ba_{0.6}Sr_{0.4}TiO_3$) thin films with different grain sizes have been successfully fabricated as metal–insulator–metal (MIM) capacitors. The perovskite structure of the material has been confirmed via X-ray diffraction (XRD). In order to correlate the effect of the grain size to the conduction mechanisms of these films, atomic force microscopy (AFM) results are presented. The grain size shows an important effect on the conduction mechanism for the films. The results show that as the grain size increases, both the impedance and the permittivity of the films decrease, whereas the conductivity shows an inverse variation. The Z^* plane for all films shows two regions, corresponding to the bulk mechanism and the distribution of the grain boundaries–electrodes conduction process. M'' versus frequency plots reveal non-Debye relaxation peaks, which are not able to be observed in the ε'' plots. Alternating current (AC) conductivity versus frequency plots show three regions of conduction processes, i.e. a low-frequency region due to direct current (DC) conduction, a mid-frequency region due to translational hopping motion, and a high-frequency region due to localized hopping and/or reorientational motion.

Key words: Barium Strontium Titanate (BST) Thin Film; Grain Size; Grain Boundaries; Impedance; Dielectric Properties; AC Conductivity.

1. Introduction

Ferroelectric materials have been extensively studied in their thin film form, mainly for application as multilayer ceramic capacitors and dynamic random access memories. Among numerous ferroelectrics, barium strontium titanate ($Ba_xSr_{1-x}TiO_3$) or BST in thin film form is considered to be one of the leading candidates for microelectronic devices due to its low-cost synthesis, high dielectric constant, low dielectric loss, and composition dependent Curie temperature, which can be controlled by adjusting the barium-to-strontium ratio [1, 2].

The grain size plays a significant role in determining the electrical properties of the polycrystalline materials [3], since they are related directly to the grain boundaries area. Furthermore, the grain boundaries mainly affect on the conduction mechanism and the relaxation phenomenon of the material, thus it is necessary to separate the conductivity due to grain boundaries from that of the bulk [4]. Impedance spectroscopy has been proven to be a powerful technique to study many of the electrical properties of materials and the contribution of the bulk, the grain boundaries, and the electrodes interface regions on the dielectric relaxation phenomenon [5 – 7]. Relatively few studies employ the impedance spectroscopy to study BST in thin film form. Czekaj et al. reported the impedance behaviour of homogeneous $Ba_{0.6}Sr_{0.4}TiO_3$ and inhomogeneous BST thin films on a stainless steel substrate [6]. Agarwal et al. studied the electrical conduction of BST in metal–insulator–semiconductor (MIS) structure under humid conditions [8]. In a previous work, the frequency dependence of the electrical properties of $Ba_{0.8}Sr_{0.2}TiO_3$ thin films has been studied using an impedance spectroscopy [9].

In this work, the effect of the grain size on the conduction mechanism of $Ba_{0.6}Sr_{0.4}TiO_3$ thin films has been studied. To obtain films with different grain sizes, films of different thicknesses have been prepared. In order to correlate the grain size with the conduction mechanism of the films, impedance, permittivity, electric modulus, and AC conductivity frequency dependent plots have been presented. The measurements are

performed using impedance/gain-phase analyzer in the frequency range of 1 Hz – 1 MHz at room temperature.

2. Experiment

A $Ba_{0.6}Sr_{0.4}TiO_3$ solution was prepared using barium acetate, strontium acetate, and titanium(IV) isopropoxide as starting material. The preparation details for the solution can be found somewhere else [10]. The solution was deposited on $Pt/SiO_2/Si$ substrate by spin-coating at 5000 rpm for 20 s, followed by baking at 200 °C for 20 min and heating at 500 °C for 30 min to vapourize the organic solvent. The deposition and heating processes were repeated until three samples A, B, and C of different thicknesses are obtained. Finally, the films were annealed at 800 °C for one hour in oxygen atmosphere.

The crystallization of the material was determined using a X-ray diffractometer (XRD), with a CuKα radiation source ($\lambda = 1.54$ Å), operated at a voltage of 40 KV and a current of 40 mA. The surface morphology of the films was investigated using an atomic force microscope (AFM) (SPA400, SII Nanotechnology Inc.), operated in contact mode. The metal-ferroelectric-metal (MFM) configuration was used for the dielectric measurement with $7.85 \cdot 10^{-3}$ cm^2 aluminium dots as a top electrode. The impedance and dielectric measurements were performed using an impedance gain/phase analyzer (Solartron 1260) in the frequency range of 10 Hz to 1 MHz at room temperature.

3. Results and Discussion

3.1. Microstructure Analysis

X-ray diffraction patterns for $Ba_{0.6}Sr_{0.4}TiO_3$ are shown in Figure 1. It can be observed from the figure that the diffraction peaks are (1 0 0), (1 1 0), (1 1 1), (2 0 0), (2 1 0), and (2 1 1) within the 2θ range from 20° to 60°, furthermore, the measured a-axis and c-axis lattice parameters are equal, $a = c = 3.965$ Å, indicating that the film is crystallized with the cubic structure phase.

In order to measure the films' thickness, the films were partially dipped in a diluted hydrofluoric acid (HF) and the resulting step-profile thickness was measured with a profilometer. The thickness of Sample A, Sample B, and Sample C are found to be 180 nm, 234 nm, and 450 nm, respectively. To obtain consistent results for the AFM, each sample was subjected to three different scanned positions of an 1 µm × 1 µm area, as shown in Figure 2. The micrographs show a good quality surface. The average of the grain size for Sample A, Sample B, and Sample C were measured to be 79 nm, 102.4 nm, and 145.8 nm, respectively. This indicates that the grain size increases as the film thickness increases. The increment of the grain size can be explained by considering the grain growth during the deposition and annealing process of the layers. During the deposition process the films were heated at 500 °C for 30 min after each layer. This temperature was enough to grow the BST grains, so the next layer deposition was carried out over films with established grain boundaries and the solution was spread over all these grains randomly. Thus bigger grains were obtained after the heating and annealing of the new layer [10].

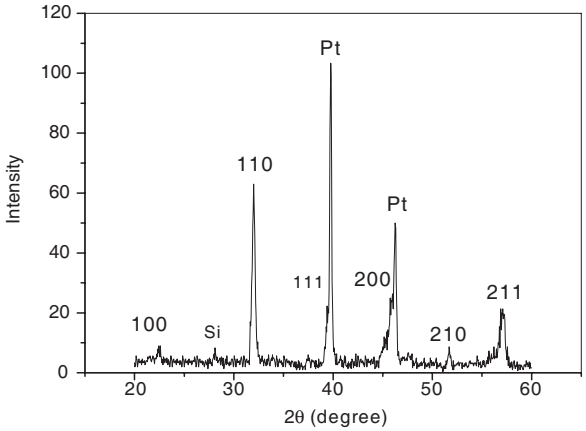

Fig. 1. XRD patterns for $Ba_{0.6}Sr_{0.4}TiO_3$.

3.2. Electric and Dielectric Measurements

The complex impedance $Z^*(f)$ of the BST system can be described by the following equation:

$$Z^*(f) = Z'(f) + iZ''(f), \tag{1}$$

where Z' and Z'' represent the real and imaginary part of the impedance, respectively. The variation of Z' and Z'' with frequency for the films used in this work is given in Figures 3a and 3b. The magnitude of Z' decreases with the increase in both frequency and film

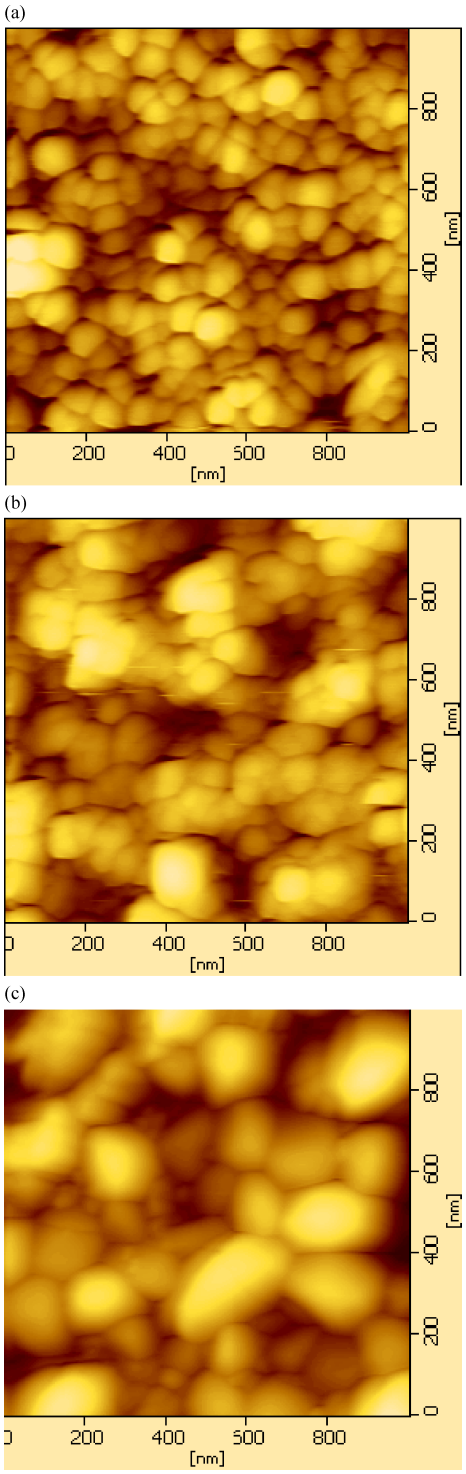

Fig. 2 (colour online). AFM micrograph for (a) Sample A, (b) Sample B, and (c) Sample C.

thickness, indicating an increase in the AC conductivity of the material, and then all curves merge at frequencies $> 10_3$ Hz to attain a constant value. Furthermore, the variation of Z'' with frequency reveals that the Z'' values reach a maximum $Z''_{\max}$, showing a peak. Such behaviour indicates the presence of relaxation in the system. Moreover, the peak maximum $Z''_{\max}$ decreases as the film thickness increase, indicating an increase in the conductivity.

In order to obtain full understanding for the effect of film regions on the conduction mechanism for the films used in this work, a Nyquist plot (Z' vs. Z'') is used as shown in Figure 4. All the films show two regions: a semicircular arc at the high frequencies region attributed to the electrical properties of the films' bulk and a depressed semicircle attributed to the grain boundaries and electrodes processes contribution to the polarization mechanism. It is observed that the bulk arc and the grain boundaries–electrode semicircle are more distinguishable for thicker films, which could be attributed to the grain size effect.

From Figures 3 and 4, it can be observed that the total impedance of the films decreases as the film thickness increases, which is attributed to the grain size effect. The increment in the bulk and grain boundaries resistance is attributed to the conduction mechanism at the grain–grain boundaries. During the heat treatment for the films in an oxygen atmosphere, oxygen atoms accumulate at the interfaces, creating many electron traps at the grain boundaries surfaces [11]; as a result, the interfaces trap electrons from the adjacent grains. This electrons cross over the grain barrier and flow into the grain boundary layers, filling the traps first and then accumulating at the grain boundary interfaces forming a space charge [11, 12]. However, as the grain size decreases, the number of charge carriers reduces due to the continued electron loss to the grain boundaries. Furthermore, the AFM results show that Sample A has the smallest grains; therefore, it has the highest resistance. Hence, as the grain size decreases the area of the grain boundaries and electrode interfaces increase [13, 14], and this leads to an increase in the grain boundaries–electrode resistance due to the increase of the space charge density.

The study of the dielectric properties is another important source of valuable information about conduction processes since it can be used to understand the origin of dielectric losses and electrical and dipolar relaxation time [15]. For this matter, the dielectric per-

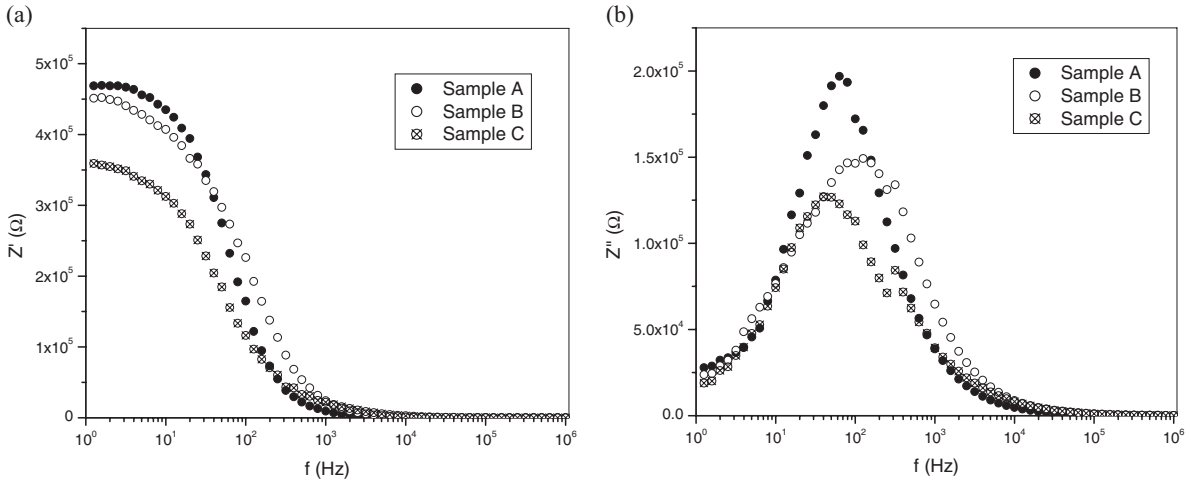

Fig. 3. Variation of (a) Z' and (b) Z'' as a function of frequency for Sample A, Sample B, and Sample C.

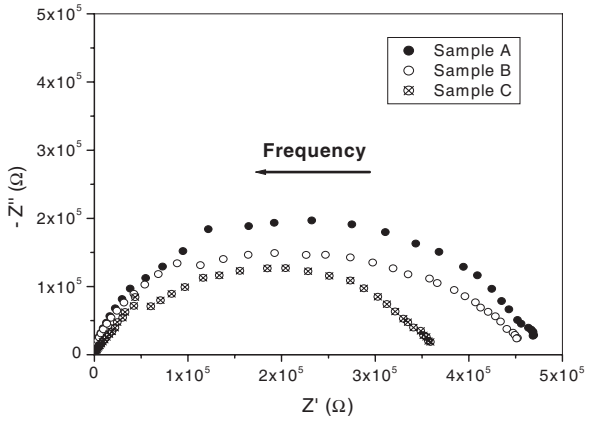

Fig. 4. Nyquist plots for Sample A, Sample B, and Sample C.

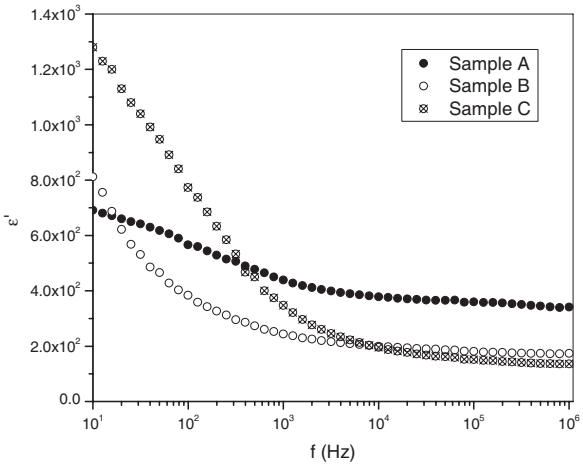

Fig. 5. Variation of the ε' versus frequency for Sample A, Sample B, and Sample C.

mittivity and the electric modulus were determined from the measured values of the impedance using the following relations [16]:

$$\varepsilon^* = \varepsilon' - \mathrm{i}\varepsilon'' = \frac{-Z'}{(Z'^2 + Z''^2)\omega C_o} + \frac{-Z''}{(Z'^2 + Z''^2)\omega C_o} \quad (2)$$

and [17]

$$M^* = (\varepsilon^*)^{-1} = M' - \mathrm{i}M'' = \frac{\varepsilon'}{(\varepsilon'^2 + \varepsilon''^2)} - \frac{\varepsilon''}{(\varepsilon'^2 + \varepsilon''^2)}, \quad (3)$$

where ε' and ε'' are the real and imaginary components of the dielectric permittivity, respectively, whereas M' and M'' are the components of the electric modulus.

Figure 5 shows the variation of ε' with the frequency for tested films at room temperature. It is observed that the value of ε' for all the films decreases as the frequency increases and attains a constant limiting value, at which ε' becomes almost frequency independent. The high value of the dielectric constant at low frequencies can be explained as an accumulation of charges at the interfaces between the sample and the electrodes, i.e., Maxwell–Wagner polarization and interfacial polarization [18]. As the frequency increases, the dipoles in the samples can not reorient themselves fast enough to respond to the applied electric field resulting in the decrease of ε'.

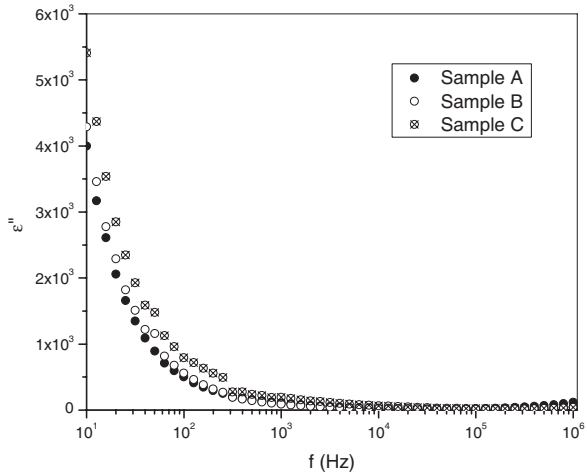

Fig. 6. Variation of ε'' versus frequency for Sample A, Sample B, and Sample C.

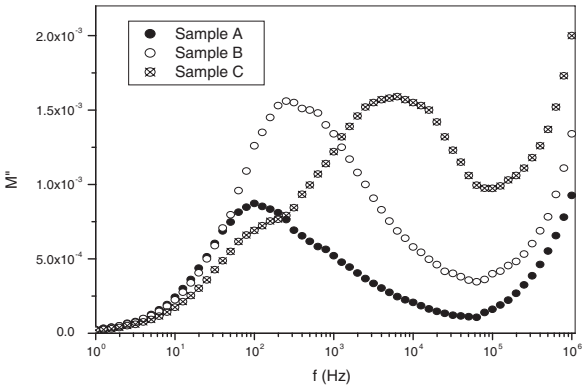

Fig. 7. Variation of M'' versus frequency for Sample A, Sample B, and Sample C.

On the other hand, at higher frequencies, it has been observed that the ε' value increase as the film thickness decreases, which is attributed to the decrease in grain sizes. AFM results show that the thinner films have smaller grain sizes, which implies a larger grain boundaries area. However, it can be considered that the grains and the grain boundaries act as interior capacitors network, since the grains are more conducting compared to the grain boundaries [19]. This implies that the effective capacitance of the film increases with the grain size decrease, due to the increase of the grain boundaries area. As a result, the overall dielectric constant of the film increases with grain size decrease.

Figure 6 shows the frequency dependence of the imaginary part of the dielectric constant (dielectric loss) ε'' for Sample A, Sample B, and Sample C films at room temperature. Similar features for dielectric loss are observed as for dielectric constant. There are no appreciable relaxation peaks observed in the frequency range employed in this study. It is believed that the ionic conduction may mask any relaxation mechanism.

In order to reveal the relaxation peak in the ε'' plot, the effect of electrode polarization must be excluded. This can be achieved by following the electric modulus approach, since the electric modulus corresponds to the relaxation on the electric field in the material when the electric displacement remains constant. This approach can be effectively used to separate out the electrode effects which mask the dielectric relaxation. Figure 7 shows M'' versus frequency plots for Sample A, Sample B, and Sample C. For Sample A and Sample B, M'' shows a broad and asymmetric peak located in the range of ~ 50 Hz to ~ 2 kHz. The maximum of this peak shifts toward higher frequencies as the film thickness increases. In Sample C, a broad peak is noticed at low frequencies ~ 70 Hz and a well-defined peak at medium frequencies ~ 6.4 kHz. The frequency range where the peak occurs in the M'' plot indicates the transition from long range to short range mobility [13, 20].

The modulus plot can be characterized by full width at half maximum (FWHM) or in terms of a non-exponential decay function. The stretched exponential function is defined by the empirical Kohlrausch–Williams–Watts (KWW) relationship [13, 20]

$$\phi(t) = \mathrm{e}^{(-t/\tau)^{\beta}}, \quad 0 < \beta < 1, \tag{4}$$

where τ is the characteristic relaxation time and β the Kohlrausch parameter, which represents the deviation from a Debye-type relaxation ($\beta = 1$) and decreases with the increasing of the relaxation time distribution.

The value of parameter β is calculated by extracting FWHM of the modulus peaks using $\beta = 1.14/\mathrm{FWHM}$. It has been found that the values of β for Sample A, Sample B, and Sample C films are 0.57, 0.76, and 0.87, respectively. This indicates that the relaxation process for all the tested samples is of non-Debye type. Furthermore, the smaller the value of β, the greater the deviation with respect to Debye type relaxation [21]. However, the low frequency peak in Sample C film is considered to be a non-Debye peak also since it is too broad.

The study of frequency dependent conductivity is a well established method for characterizing the hop-

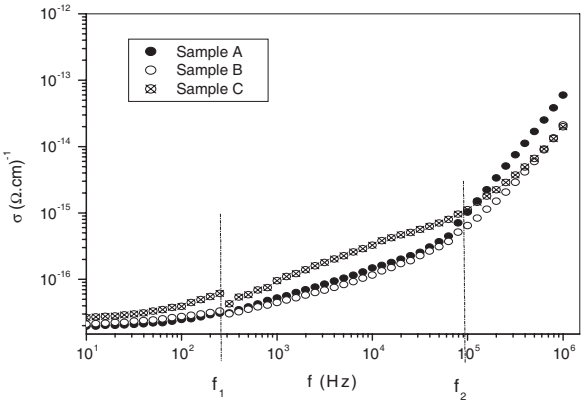

Fig. 8. AC conductivity as a function of frequency for Sample A, Sample B, and Sample C.

ping dynamics of the charge carrier/ions [11]. Figure 8 shows the typical frequency dependence of AC conductivity (σ_{AC}) for various film thicknesses. The frequency dependence of AC conductivity is usually characterized by a power law as given below [22–24]:

$$\sigma_{AC} = Af^n, \tag{5}$$

where A is a temperature dependent constant and n is the frequency exponent, which can be determined from the measured results.

It is observed from Figure 8 that all films show two threshold frequencies, f_1 and f_2, separating the entire variation into three regions: (i) Low frequencies region, $f < f_1$, in which the conductivity is almost frequency independent, called σ_{DC}. (ii) Moderate frequencies region, $f_1 < f < f_2$. The conductivity increases linearly with the frequency. The values of n are obtained by fitting σ versus f plots in this region, which are found to be located between 0.51 and 0.53, i.e. $0 < n < 1$. This reveals that the conduction mechanism in this region corresponds to the translational hopping motion [23, 24]. (iii) High frequencies region, $f > f_2$. The conductivity increases linearly with the frequency. In this region the n values vary between 1.26 and 1.75, i.e. $1 < n < 2$. This reveals that the conduction mechanism in this rang of frequency corresponds to the well localized hopping and/or reorientational motion [22, 23].

It is also observed from Figure 8 that the conductivity increases as the film thickness increases; this is attributed to the grain size effect. AFM results show that the films of less thickness have smaller grains, which leads to a larger grain boundaries area. This in turn gives rise to higher density of the charges accumulated at the interfaces. These charges act as to block any mobility for the free carrier, thus, the conductivity of the film decreases as a result. These results agree very well with the impedance results in Figures 3 and 4.

4. Conclusion

Perovskite-type $Ba_{0.6}Sr_{0.4}TiO_3$ thin films with different grain sizes of 79 nm, 102.4 nm, and 145.8 nm have been successfully fabricated as MIM capacitors using sol-gel technique. The grain size shows an essential effect on the conduction mechanism for the films. The results show that as the grain size increases, the impedance and the permittivity of the films decrease, whereas the AC conductivity shows an inverse variation. The Z^* plane for all the films shows two regions, corresponding to the bulk mechanism and the distribution of the grain boundaries–electrodes conduction process. M'' versus frequency plots reveal non-Debye relaxation peaks, which are not able to be observed in ε'' plots. AC conductivity versus frequency plots show three regions of conduction processes, i.e. a low-frequency region due to DC conduction, a mid-frequency region due to translational hopping motion, and a high-frequency region due to localized hopping and/or reorientational motion.

[1] C. Fu, C. Yang, H. Chen, L. Hu, and Y. Wang, Mater. Lett. **59**, 330 (2005).
[2] T. Mazon, M. A. Zaghete, J. A. Varela, and E. Longo, J. Eur. Ceram. Soc. **27**, 3799 (2007).
[3] A. Tschope, Solid State Ionic. **139**, 267 (2001).
[4] K. Prabakar, S. K. Narayandass, and D. Mangalaraj, Mater. Sci. Eng. B **98**, 225 (2003).
[5] J. C. C. Abrantes, J. A. Labrincha, and J. R. Frade, Mater. Res. Bull. **35**, 727 (2000).
[6] D. Czekaj, A. Lisinska-Czekaj, T. Orkisz, J. Orkisz, and G. Smalarz, J. Eur. Ceram. Soc. **30**, 465 (2010).
[7] I. F. Al-Hamarneh, P. D. Pedrow, S. C. Goheen, and M. J. Hartenstine, IEEE Trans. Plasma Sci. **35**, 518 (2007).
[8] S. Agarwal, G. L. Sharma, and R. Manchanda, Solid State Commun. **119**, 681 (2001).
[9] A. A. Saif, Z. A. Z. Jamal, Z. Sauli, and P. Poopalan, Mater. Sci. (Medžiagotyra) **17**, 186 (2011).

[10] A. A. Saif and P. Poopalan. Solid State Electron. **62**, 25 (2011).
[11] L. Bing-Ce, L. Ci-Hui, F. Zhu-Xi, and Y. Bo, Chin. Phys. Lett. **26**, 117101 (2009).
[12] A. Alim Mohammad, S. Li, F. Liu, and P. Cheng, Phys. Status Solidi (a) **203**, 410 (2005).
[13] C. Qingheng, H. Jinliang, T. Kexiong, C. Shuiming, Y. Minyu, and T. Jianxin, Sci. Chin. (E) **45**, 337 (2002).
[14] S. C. Roya, G. L. Sharma, M. C. Bhatnagar, R. Manchanda, V. R. Balakrishnan, and S. B. Samanta, Appl. Surf. Sci. **236**, 306 (2004).
[15] R. Ayouchi, D. Leinen, F. Martın, M. Gabas, E. Dalchiele, and J. R. Ramos-Barrado, Thin Solid Films. **426**, 68 (2003).
[16] D. K. Pradhan, R. N. P. Choudhary, and B. K. Samantaray, Int. J. Electrochem. Sci. **3**, 597 (2008).
[17] E. Arslan, Y. Safak, I. Tascoglu, H. Uslu, and E. Ozbay, Microelectron. Eng. **87**, 1997 (2010).
[18] U. Akgul, Z. Ergin, M. Sekerci, and Y. Atici, Vacuum **82**, 340 (2008).
[19] A. A. Saif and P. Poopalan. J. Korean Phys. Soc. **57**, 1449 (2010).
[20] P. S. Anantha and K. Hariharan, Mater. Sci. Eng. B **121**, 12 (2005).
[21] M. Ram and S. Chakrabarti, J. Alloys Compd. **462**, 214 (2008).
[22] S. Mahboob, G. Prasad, and G. S. Kumar, Bull. Mater. Sci. **29**, 347 (2006).
[23] A. Oueslati, F. Hlel, K. Guidara, and M. Gargouri, J. Alloys Compd. **492**, 508 (2010).
[24] P. Muralidharan, M. Venkateswarlu, and N. Satyanarayana, Mater. Chem. Phys. **88**, 138 (2004).